Article

Cell Systems

Chaotic Dynamics Mediate Brain State Transitions, Driven by Changes in Extracellular Ion Concentrations

Graphical Abstract

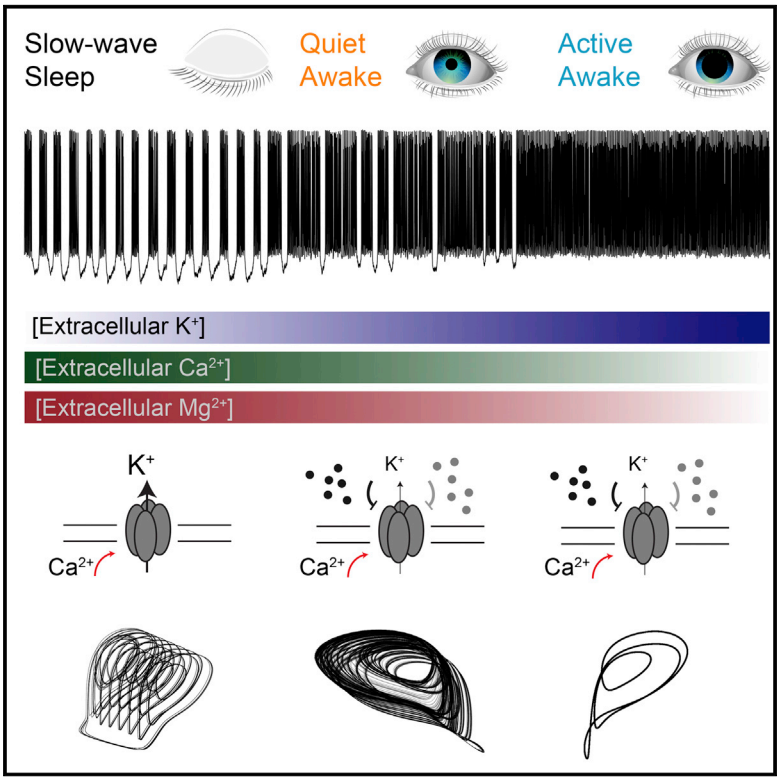

Authors

Rune Rasmussen, Mogens H. Jensen, Mathias L. Heltberg

Correspondence

runerasmussen@dandrite.au.dk (R.R.), heltberg@nbi.ku.dk (M.L.H.)

In Brief

By extending the Averaged-Neuron model to include changes in extracellular ion concentrations, Rasmussen et al. show that transitions between states of sleep and wakefulness are facilitated by ionic changes and governed by chaotic dynamics, which ensure smooth and robust transitions.

Highlights

- The Averaged-Neuron model is extended to include extracellular ionic changes
- *In vivo* sleep- and wake-dependent neuronal firing patterns are recapitulated
- Extracellular ionic changes lower the threshold for transitioning to wakefulness
- Chaotic dynamics create a smooth transition between different activity states

Rasmussen et al., 2017, Cell Systems *5*, 591–603
December 27, 2017
https://doi.org/10.1016/j.cels.2017.11.011

CellPress

Cell Systems
Article

Chaotic Dynamics Mediate Brain State Transitions, Driven by Changes in Extracellular Ion Concentrations

Rune Rasmussen,[1,3,*] Mogens H. Jensen,[2] and Mathias L. Heltberg[2,3,4,*]
[1]The Danish Research Institute of Translational Neuroscience – DANDRITE, Nordic EMBL Partnership for Molecular Medicine, Department of Biomedicine, Aarhus University, 8000 Aarhus C, Denmark
[2]Niels Bohr Institute, University of Copenhagen, 2100 Copenhagen, Denmark
[3]These authors contributed equally
[4]Lead Contact
*Correspondence: runerasmussen@dandrite.au.dk (R.R.), heltberg@nbi.ku.dk (M.L.H.)
https://doi.org/10.1016/j.cels.2017.11.011

SUMMARY

Previous studies have suggested that changes in extracellular ion concentrations initiate the transition from an activity state that characterizes sleep in cortical neurons to states that characterize wakefulness. However, because neuronal activity and extracellular ion concentrations are interdependent, isolating their unique roles during sleep-wake transitions is not possible *in vivo*. Here, we extend the Averaged-Neuron model and demonstrate that, although changes in extracellular ion concentrations occur concurrently, decreasing the conductance of calcium-dependent potassium channels initiates the transition from sleep to wakefulness. We find that sleep is governed by stable, self-sustained oscillations in neuronal firing patterns, whereas the quiet awake state and active awake state are both governed by irregular oscillations and chaotic dynamics; transitions between these separable awake states are prompted by ionic changes. Although waking is indicative of a shift from stable to chaotic neuronal firing patterns, we illustrate that the properties of chaotic dynamics ensure that the transition between states is smooth and robust to noise.

INTRODUCTION

During transition from sleep to awake, the brain passes from a state that attenuates sensory inputs to one that often amplifies them (Lee and Dan, 2012; McGinley et al., 2015b; Polack et al., 2013). How this transition between states occurs is still incompletely understood, both at the level of the brain and at the level of the neurons that must implement the transition in a smooth and robust way.

Cortical neurons are known to exhibit three distinct physiological and behavioral states that characterize the transition from sleep to active wakefulness. Specifically, slow-wave sleep is characterized by oscillating periods of synaptic barrages (also called "upstates") and silence ("downstates") (Steriade et al., 2001). It is understood that this behavior reflects oscillations in membrane potential (V_m) and therefore the neuron's susceptibility to input. In wakefulness, these downstates are suppressed and V_m is maintained closer to threshold. Although the classic view holds that oscillations are restricted to slow-wave sleep, recent studies have demonstrated that a quiet awake state is also characterized by low-frequency V_m oscillations. Once actively awake, however, movement and arousal suppress these oscillations, and V_m is depolarized tonically, making neurons sensitive to inputs and prone to firing. Despite our understanding of the neuronal behaviors that are indicative of transitions from slow-wave sleep to quiet awake to active awake, the underlying mechanisms that initiate these transitions remain unclear.

Recently it was proposed that changes in extracellular ion concentrations ($[K^+]_o$, $[Ca^{2+}]_o$, and $[Mg^{2+}]_o$) control activity patterns during sleep and wakefulness, and that ionic changes are sufficient to shift the state from sleep to awake (Ding et al., 2016). However, given that changes in neural activity also strongly affect extracellular ion concentrations (Amzica et al., 2002; Hounsgaard and Nicholson, 1983; Lux, 1974; Lux and Neher, 1973; Nicholson et al., 1977), it is not possible to unequivocally distinguish cause and consequence *in vivo*. For example, both spiking and excitatory barrages, which originate within the neuron itself, increase $[K^+]_o$ (Hounsgaard and Nicholson, 1983; Shih et al., 2013), making it difficult to experimentally assess causality. A remedy for solving this issue is modeling and simulations (Fröhlich et al., 2006; Krishnan et al., 2015; Tagluk and Tekin, 2014; Tatsuki et al., 2016). The ability to maintain parameters constant, thereby reducing variable space dimensionality, is a powerful tool for interrogating the impact of changes in both intracellular and extracellular ion concentrations on V_m dynamics and state transitions, as well as for formulating hypotheses and predictions for future experimental investigations.

An important step toward successfully modeling the neuronal dynamics in a simple manner, is the Averaged-Neuron model, which recently has been proposed (Tatsuki et al., 2016). This model is inspired by previously constructed neural-network models (Bazhenov et al., 2002; Chen et al., 2012; Compte et al., 2003; Hill and Tononi, 2005; Sanchez-Vives et al., 2010; Timofeev et al., 2000), but simplifies the enormous complexity of these by performing a mean-field approximation of a

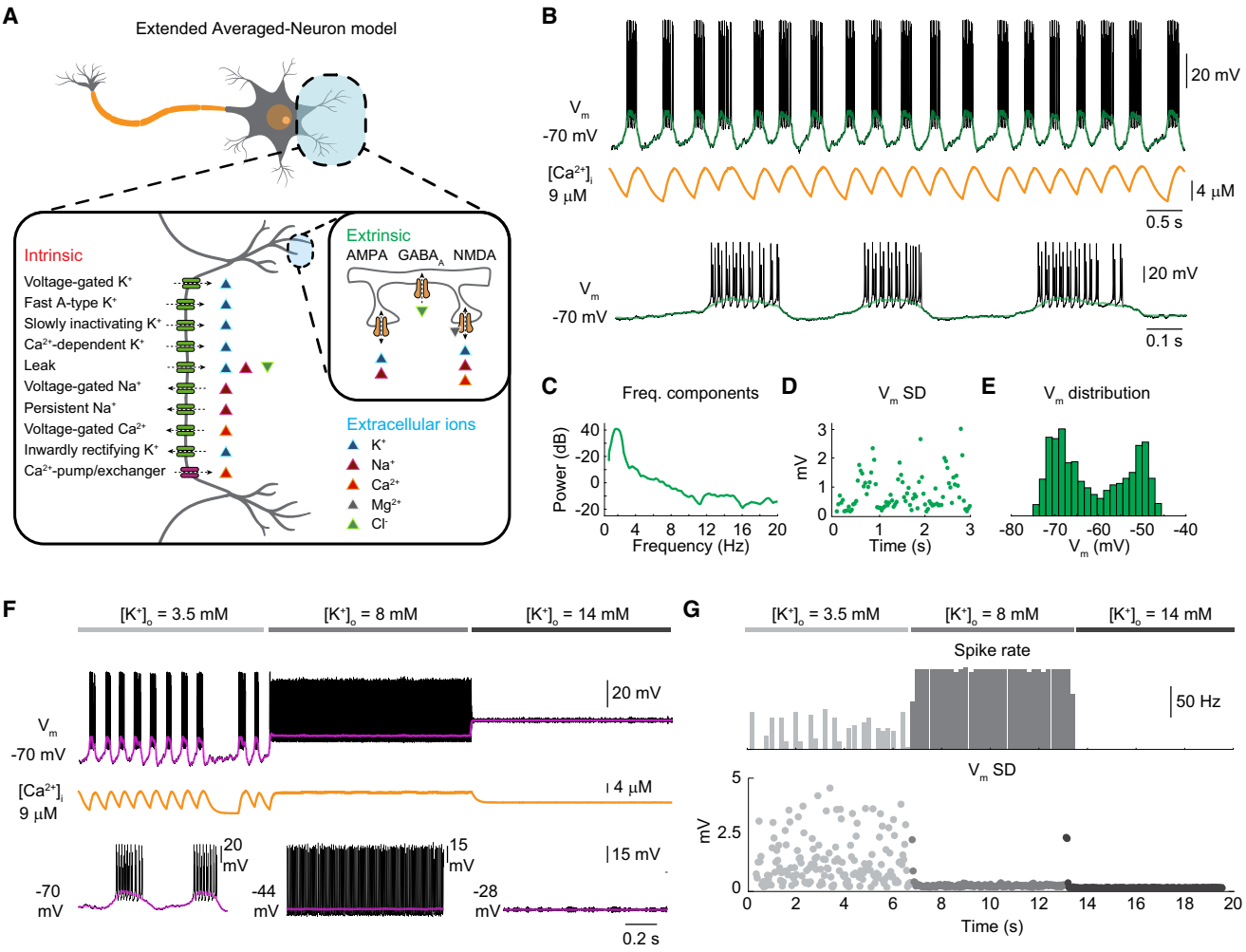

Figure 1. Implementing Ion Concentrations in the Averaged-Neuron Model

(A) Schematic diagram of the extended Averaged-Neuron model containing intrinsic ion channel conductances and Ca^{2+} pumps, extrinsic synaptic ion channel conductances, and extracellular ion concentrations.

(B) Representative slow-wave sleep membrane potential (V_m) firing pattern and intracellular Ca^{2+} concentration ($[Ca^{2+}]_i$) with the initial extracellular ion concentration parameter set ($[K^+]_o$ = 3.5 mM, $[Ca^{2+}]_o$ = 1.5 mM, and $[Mg^{2+}]_o$ = 1.1 mM). Below is an expansion of V_m dynamics.

(C) V_m frequency spectra.

(D) SD of mean V_m (spikes removed).

(E) Mean V_m distribution.

(F) Representative V_m firing pattern and $[Ca^{2+}]_i$ with 3.5, 8, or 14 mM $[K^+]_o$. Below is an expansion of V_m dynamics.

(G) Upper: Spike rate versus time for 3.5, 8, or 14 mM $[K^+]_o$. Lower: SD of mean V_m for 3.5, 8, and 14 mM $[K^+]_o$.

See also Figure S1.

population of neurons to construct an Averaged-Neuron model. The framework of the model is based on the existence of different ion channels and is mathematically described in a Hodgkin-Huxley manner; all contribute to the total change in V_m. As a first-order approximation, it is assumed that the averaged-neuron can interact with itself (directly or indirectly) through excitatory or inhibitory synaptic currents. Furthermore, intrinsic currents exist as depolarizing Na^+ and Ca^{2+} currents and hyperpolarizing K^+ currents. This polarization affects the V_m through nine different intrinsic channels (Figure 1A).

Here, we extend the Averaged-Neuron model to explicitly treat the changes in extracellular ion concentrations that occur during the sleep-wake cycle. We demonstrate how decreasing the conductance of the Ca^{2+}-dependent K^+ channel, in combination with physiological changes in $[K^+]_o$, $[Ca^{2+}]_o$, and $[Mg^{2+}]_o$, initiates state transitions in neuronal firing patterns. We find that sleep is dominated by a stable limit cycle, resulting in self-sustained, stable firing patterns, whereas wakefulness is governed by irregular oscillations and chaotic dynamics. As the ion concentrations are changed, the firing patterns become more dominated by long high-frequency upstate periods, and we predict that a state change from quiet to active awake can be induced by subtle changes in extracellular ion concentrations. Finally, we discuss how the fundamental properties of chaotic dynamics can ensure smooth transitions between brain states in the presence of intrinsic noise.

RESULTS

Implementing Dynamic Ion Concentration Dependencies in the Averaged-Neuron Model

As a starting point for investigating the influence of extracellular ion concentrations on neuronal states, we first implemented and extended the Averaged-Neuron model (Tatsuki et al., 2016). In this model, a single neuron feeds back onto itself directly and indirectly, through synaptic excitatory and inhibitory conductances (AMPA, NMDA, and $GABA_A$ receptors) (Figure 1A). In addition to synaptic conductances, the Averaged-Neuron model includes the following intrinsic conductances, either depolarizing or hyperpolarizing V_m: voltage-gated (Na_V) and persistent (NaP) Na^+ channels, voltage-gated (Ca_V) Ca^{2+} channels, voltage-gated (K_V), leak (K_{Leak}), fast A-type ($K_{A\text{-}type}$), inwardly rectifying (K_{IR}), slowly inactivating (K_{SI}), and Ca^{2+}-dependent (K_{Ca}) K^+ channels, and finally a Ca^{2+}-pump/exchanger expelling Ca^{2+} ions from the intracellular compartment (Tatsuki et al., 2016) (Figure 1A). For all of these conductances, we adapted the full parameter set from the original Averaged-Neuron model published by Tatsuki et al. (2016). The original Averaged-Neuron model did not consider changes in extracellular ion concentrations as variables but as fixed constants. We extended the Averaged-Neuron model by introducing extracellular and intracellular ion concentration dependencies by implementing Nernst and Goldman-Hodgkin-Katz equations for calculating reversal potentials for all receptors and channels. We also added a $[Mg^{2+}]_o$ dependency for the NMDA receptor that satisfies the criteria that higher $[Mg^{2+}]_o$ leads to lower current (Mayer et al., 1984; Nowak et al., 1984) (Figure 1A). A detailed formal description of the extended Averaged-Neuron model is provided in the STAR Methods and the code is available on GitHub (https://github.com/Neurune/IonsAndChaos).

First, we simulated V_m in time with an initial extracellular ion concentration parameter set of $[K^+]_o = 3.5$ mM, $[Ca^{2+}]_o = 1.5$ mM, and $[Mg^{2+}]_o = 0.8$ mM. The remaining intra- and extracellular ion concentrations were maintained constant, and values were based on previous *in vivo* and *in vitro* experimental measurements (Diarra et al., 2001; Dietzel et al., 1982; Markova et al., 2008; Raimondo et al., 2013; Rose and Konnerth, 2001; Rose and Ransom, 1996). We found that the model remarkably closely recapitulated previous recordings obtained from neurons during slow-wave sleep (simply referred to as sleep from here on) (Steriade et al., 2001) (Figure 1B). The extended Averaged-Neuron model generated wave forms of slow oscillatory patterns, consisting of alternating periods of V_m depolarization and spiking (upstates) and V_m hyperpolarization and silence (downstates). This oscillatory pattern was also present in the modeled intracellular Ca^{2+} concentration ($[Ca^{2+}]_i$), with upstates generating a ~8 μM rise in $[Ca^{2+}]_i$ (Figure 1B). The preferential slow V_m oscillations were evident when analyzing frequency components for ten simulations, showing a high prevalence of 1–4 Hz delta power (Figure 1C). The moving SD of the mean V_m (spikes removed) varied between 0.1 and 3 mV (Figure 1D), similar to the seminal recordings obtained by Steriade et al. (2001). Finally, mean V_m showed a clear bimodal distribution, with peaks around −70 and −50 mV, reflecting the equal presence of up- and downstates separated by ~20 mV (Figure 1E).

To assess the validity of our implemented ion concentration dependencies in the extended Averaged-Neuron model, we sought to test the effect of increasing $[K^+]_o$ from 3.5 to 8 to 14 mM. The resting V_m of neurons is mainly determined by K^+-permeable conductances, and V_m is highly sensitive to changes in $[K^+]_o$ (Fröhlich et al., 2008). Thus, we expected drastic V_m changes when pushing $[K^+]_o$ to the biological extremes if our model was valid. When increasing $[K^+]_o$ from 3.5 to 8 mM, we observed a qualitative change in V_m dynamics. The alternating up- and downstates disappeared, and instead V_m was maintained depolarized and the neuron fired continuously at rates of ~100 Hz, giving rise to a tonic elevation in $[Ca^{2+}]_i$ at ~9 μM (Figures 1F and 1G). This finding is in congruence with *in vitro* slice experiments, inducing epileptic seizure activity by increasing $[K^+]_o$ to 7.5 or 8.5 mM in the external media (Jensen and Yaari, 1997; Traynelis and Dingledine, 1988). Further elevating $[K^+]_o$ to 14 mM depolarized V_m even more but also completely abolished action potential firing, releasing the tonic $[Ca^{2+}]_i$ elevation (Figures 1F and 1G). This effect is likely explained by depolarization-induced conductance blockage, where Na_V channels are kept hostage in the inactivated configuration, resulting in the inability of the neuron to fire (De Col et al., 2008; Orkand et al., 1966). This observed effect appears similar to what is seen during *in vivo* cortical spreading depression, where $[K^+]_o$ reaches levels above 12 mM (Enger et al., 2015), leading to annihilation of neural activity in the affected brain area (Grafstein, 1956; Somjen, 2001, 2002, 2004). An example of how V_m dynamics are also modulated by extreme shifts in $[Ca^{2+}]_o$ is provided in Supplemental Information (Figure S1).

Overall, these results demonstrate that the extended Averaged-Neuron model very closely recapitulates cardinal properties of V_m dynamics during sleep and is expectedly sensitive to changes in extracellular ion concentrations.

Shifting from Sleep to Awake Ion Concentrations Induces No Apparent State Transition

It was recently suggested that changes in extracellular ion concentrations ($[K^+]_o$, $[Ca^{2+}]_o$, and $[Mg^{2+}]_o$) control state-dependent activity patterns during sleep and wakefulness, and that ion shifts are sufficient to mediate the transition from sleep to awake (Ding et al., 2016). However, due to the intimate relation between neural activity and ionic changes, establishing causality *in vivo* is non-trivial.

To investigate the effect of ion concentration changes on sleep to awake transitions in the extended Averaged-Neuron model, we used the previously measured extracellular ion concentrations during sleep ($[K^+]_o = 3.9$ mM, $[Ca^{2+}]_o = 1.35$ mM, and $[Mg^{2+}]_o = 0.8$ mM) and awake ($[K^+]_o = 4.4$ mM, $[Ca^{2+}]_o = 1.2$ mM, and $[Mg^{2+}]_o = 0.7$ mM) (Ding et al., 2016) (Figure 2A). With sleep ions, V_m dynamics closely recapitulated sleep with alternating up- and downstates. When we switched to awake ions, no apparent change in V_m dynamics was obvious, except a subtle tendency for more spikes per upstate (Figure 2B). When we analyzed V_m frequency components, we found no significant difference in 1–4 Hz delta power between sleep (21.2 ± 0.24 dB) and awake ions (20.4 ± 0.62 dB) ($p = 0.08$, Student's t test, $n = 10$ simulations) (Figures 2C and 2D). Also mean V_m SD, a frequently used indicator for neuronal state (McGinley et al., 2015a; Steriade et al., 2001; Yamashita et al.,

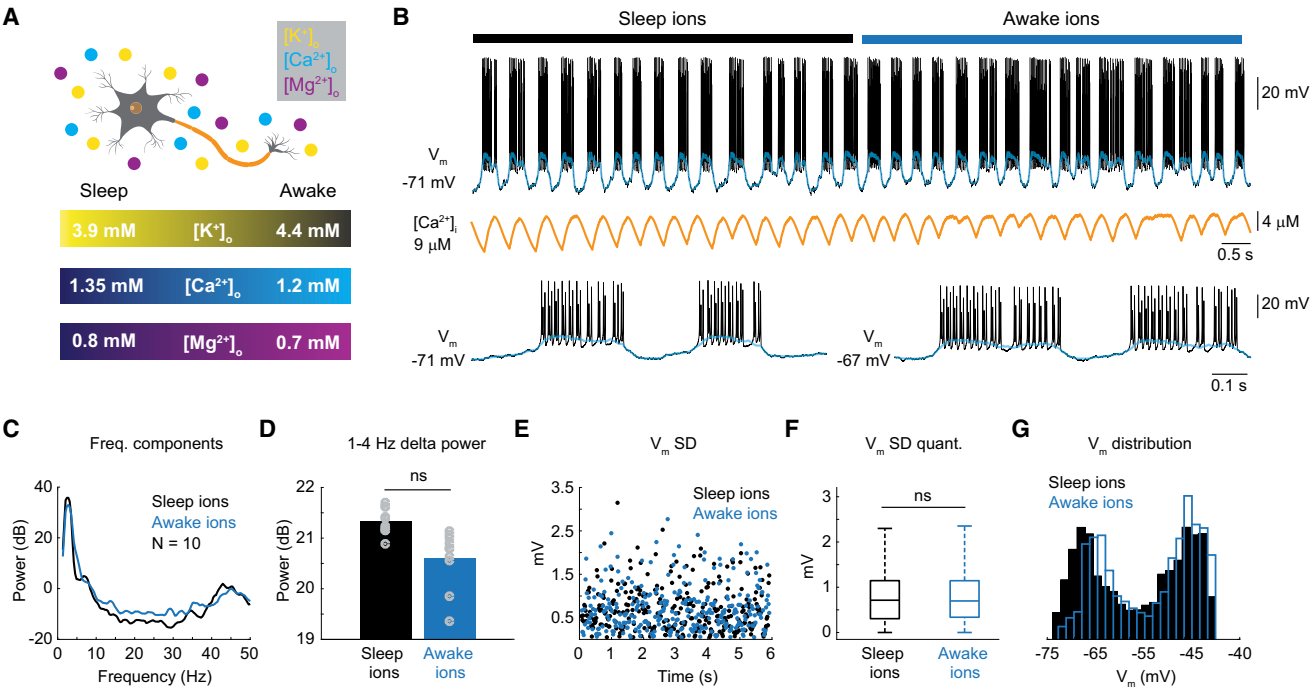

Figure 2. Shifting from Sleep to Awake Extracellular Ion Concentrations Does Not Induce State Change

(A) Schematic diagram of extracellular ion concentrations used. Sleep: $[K^+]_o$ = 3.9 mM, $[Ca^{2+}]_o$ = 1.35 mM, and $[Mg^{2+}]_o$ = 0.8 mM. Awake: $[K^+]_o$ = 4.4 mM, $[Ca^{2+}]_o$ = 1.2 mM, and $[Mg^{2+}]_o$ = 0.7 mM.

(B) Representative membrane potential (V_m) firing pattern and intracellular Ca^{2+} concentration ($[Ca^{2+}]_i$) with sleep and awake ion composition. Below is an expansion of V_m dynamics.

(C) V_m frequency spectra for sleep and awake ion composition.

(D) 1–4 Hz delta power for sleep and awake ion composition (non-significant [ns] p = 0.08, Student's t test, n = 10 simulations).

(E) SD of mean V_m (spikes removed) with sleep or awake ion composition.

(F) Boxplot for SD of mean V_m with sleep or awake ion composition. Center line is the median, box limits are 25th and 75th percentiles, and whiskers are maximum and minimum values (ns p = 0.089, Student's t test, n = 10 simulations).

(G) Mean V_m distribution with sleep or awake ion composition.

See also Figure S2.

2013), was similar for sleep (0.77 ± 0.62 mV) and awake ions (0.78 ± 0.58 mV) (p = 0.089, Student's t test, n = 10 simulations) (Figures 2E and 2F). Finally, mean V_m showed a clear bimodal distribution with both sleep and awake ion concentrations (Figure 2G).

Taken together, shifting the extracellular concentrations of K^+, Ca^{2+}, and Mg^{2+} with the same magnitude as measured *in vivo* during sleep and awake failed to induce a cortical state transition, suggesting that ion changes of this magnitude alone are not sufficient to produce a transition from sleep to awake. To exclude that these findings were not merely a special case of one parameter set, we evaluated the effect of switching from sleep to awake ion concentrations, but with varying values of model parameters. These analyses showed the same overall result, as with the initial parameter set (Figure S2) thus substantiating our initial conclusion.

Partially Inhibiting the K_{Ca} Channel Induces Sleep to Awake State Transition

Early seminal and more recent work has implicated the K_{Ca} channel in V_m activity patterns observed during sleep and wakefulness (Steriade et al., 1993; Tatsuki et al., 2016). Following a rise in $[Ca^{2+}]_i$ this channel activates and generates an outward K^+ current, hyperpolarizing V_m. In this way, the K_{Ca} channel was proposed as a key component for generating downstates during sleep (Steriade et al., 1993). In contrast, with elevated levels of neuromodulators (acetylcholine, norepinephrine, serotonin, and histamine) as seen during wakefulness (Lee and Dan, 2012), the K_{Ca} channel is partially inhibited (McCormick and Williamson, 1989; McCormick et al., 1993), and this could potentially induce the sleep to awake transition by preventing the occurrence of downstates (Steriade et al., 1993).

During our sleep V_m simulations, we observed a close relation between mean V_m and $[Ca^{2+}]_i$ oscillations with a 0.12 s lag for $[Ca^{2+}]_i$ (Figure 3A). This led us to analyze the relation between $[Ca^{2+}]_i$ and the K_{Ca} current. Not surprisingly, we found a −0.013 s lag between $[Ca^{2+}]_i$ and K_{Ca} currents (Figure 3B). The largest K_{Ca} currents occurred when mean V_m was most depolarized, and V_m rapidly hyperpolarized following peak K_{Ca} currents (Figure 3C), suggesting that K_{Ca}-mediated outward currents could be key for generating downstates.

To assess the role of the K_{Ca} channel and to mimic the elevation in neuromodulator levels seen during wakefulness (Lee and Dan, 2012; McCormick and Williamson, 1989), we reduced the

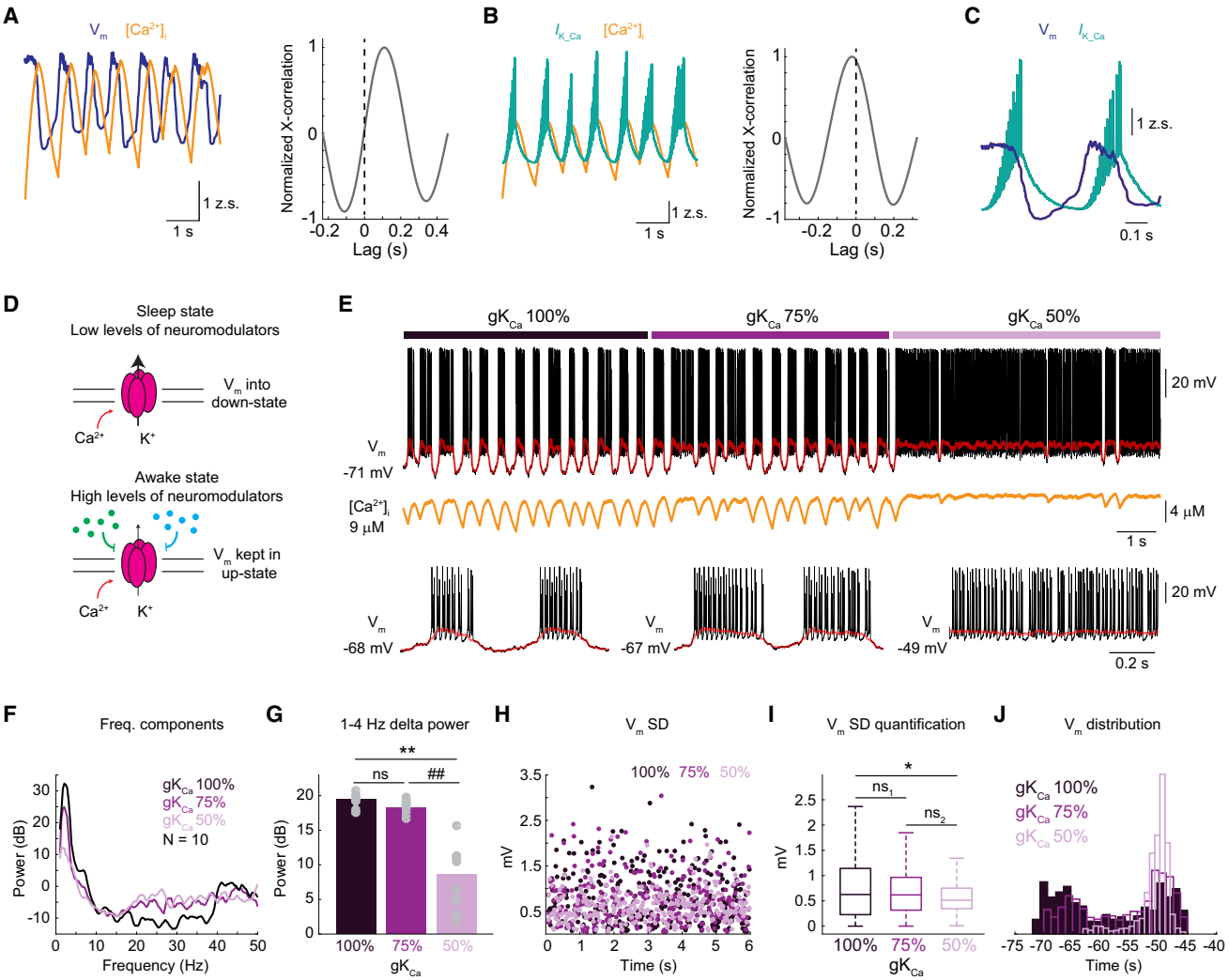

Figure 3. Partially Inhibiting Ca^{2+}-Activated K^+ Channel Can Induce Sleep to Awake State Change

(A) Left: Relation between membrane potential (V_m) and intracellular Ca^{2+} concentration ($[Ca^{2+}]_i$). Right: Cross-correlation between V_m and $[Ca^{2+}]_i$.

(B) Left: Relation between Ca^{2+}-activated K^+ channel current (I_{K_Ca}) and $[Ca^{2+}]_i$. Right: Cross-correlation between I_{K_Ca} and $[Ca^{2+}]_i$.

(C) Relation between V_m and I_{K_Ca}.

(D) Schematic diagram of speculated sleep and awake state and neuromodulator-mediated decrease of Ca^{2+}-activated K^+ channel conductance (gK_{Ca}).

(E) Representative V_m firing pattern and $[Ca^{2+}]_i$ with 100%, 75%, or 50% gK_{Ca}. Below is an expansion of V_m dynamics.

(F) V_m frequency spectra for 100%, 75%, and 50% gK_{Ca}.

(G) 1–4 Hz delta power for 100%, 75%, and 50% gK_{Ca} (non-significant [ns], p = 0.383, **p = 0.0069, ##p = 0.0083, one-way ANOVA, n = 10 simulations).

(H) SD of mean V_m (spikes removed) with 100%, 75%, and 50% gK_{Ca}.

(I) Boxplot for SD of mean V_m with 100%, 75%, and 50% gK_{Ca}. Center line is the median, box limits are 25th and 75th percentiles, and whiskers are maximum and minimum values (ns_1 p = 0.875, *p = 0.0262, ns_2 p = 0.065, one-way ANOVA, n = 10 simulations).

(J) Mean V_m distribution for 100%, 75%, and 50% gK_{Ca}.

See also Figure S3.

conductance of the K_{Ca} channel (gK_{Ca}) over time (100% = 2.3 mS/cm^2, 75% = 1.73 mS/cm^2, and 50% = 1.15 mS/cm^2). This simulation was performed with the sleep ion concentrations being maintained throughout. When reducing gK_{Ca} to 75%, we observed only a tendency toward a state change, with longer upstates and fewer downstates, whereas reducing gK_{Ca} to 50% produced a clear state change, almost completely preventing V_m from entering downstates, thereby producing tonic firing (Figure 3E). This qualitative interpretation was supported when quantified. Decreasing gK_{Ca} to 75% non-significantly reduced 1–4 Hz delta power (p = 0.383, one-way ANOVA, n = 10 simulations), whereas 50% significantly reduced delta power (p = 0.0069, one-way ANOVA, n = 10 simulations). Mean V_m SD was similar between 100% (0.74 ± 0.55 mV) and 75% gK_{Ca} (0.67 ± 0.46 mV) (p = 0.875, one-way ANOVA, n = 10 simulations), but significantly reduced with 50% gK_{Ca} (0.59 ± 0.32 mV) (p = 0.0262, one-way ANOVA, n = 10 simulations) (Figures 3H and 3I). Finally, mean V_m distributions for 100% and 75% gK_{Ca} appeared bimodal, whereas the 50% gK_{Ca} distribution was uni-modal (Figure 3J).

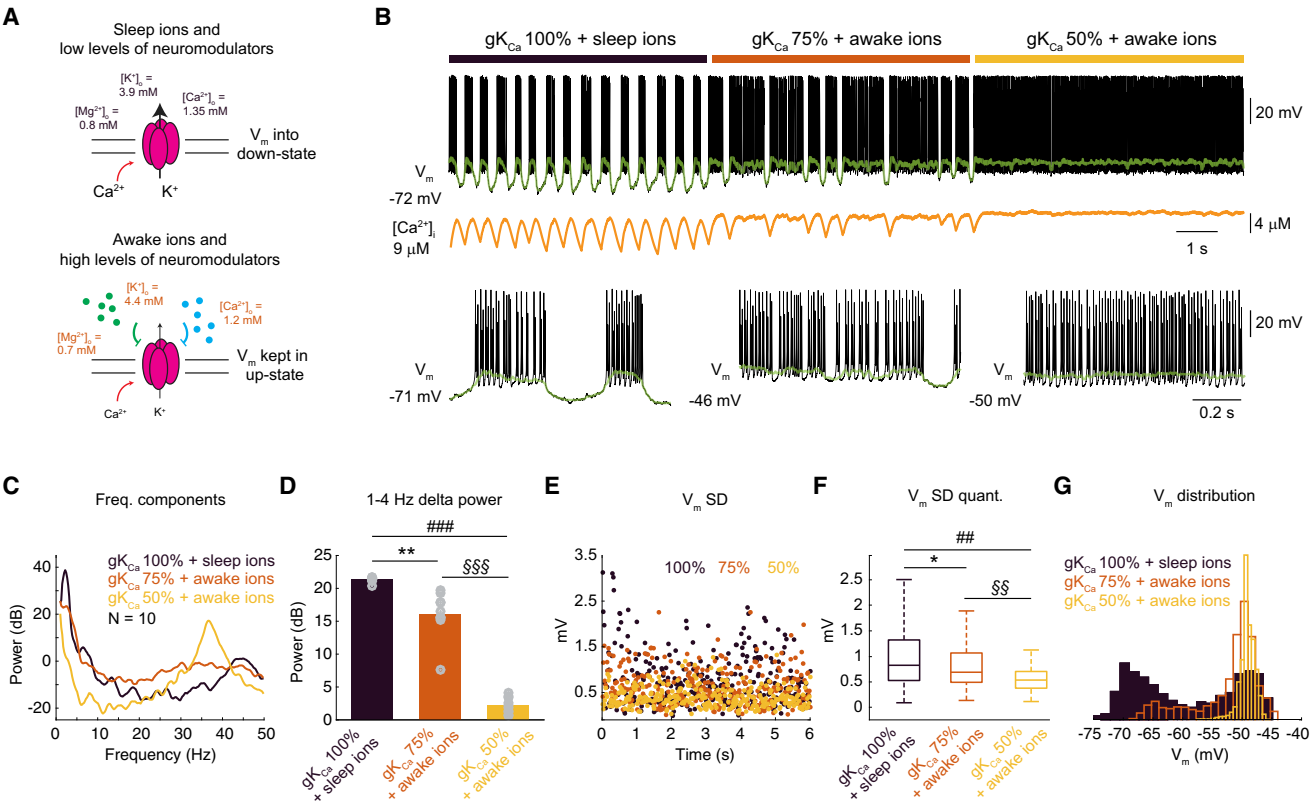

Figure 4. Awake Ion Concentrations Lowers the Threshold for Sleep to Awake State Change

(A) Schematic diagram of speculated interaction between extracellular ion concentrations, neuromodulators, and Ca^{2+}-activated K^+ channel conductance (gK_{Ca}) during sleep and wakefulness.

(B) Representative membrane potential (V_m) firing pattern and intracellular Ca^{2+} concentration ($[Ca^{2+}]_i$) with 100% gK_{Ca} + sleep ions ($[K^+]_o$ = 3.9 mM, $[Ca^{2+}]_o$ = 1.35 mM, and $[Mg^{2+}]_o$ = 0.8 mM), 75% gK_{Ca} + awake ions ($[K^+]_o$ = 4.4 mM, $[Ca^{2+}]_o$ = 1.2 mM, and $[Mg^{2+}]_o$ = 0.7 mM) or 50% gK_{Ca} + awake ions. Below is an expansion of V_m dynamics.

(C) V_m frequency spectra for 100% gK_{Ca} + sleep ions, 75% gK_{Ca} + awake ions, or 50% gK_{Ca} + awake ions.

(D) 1–4 Hz delta power for 100% gK_{Ca} + sleep ions, 75% gK_{Ca} + awake ions, or 50% gK_{Ca} + awake ions (**p = 0.026, $^{###}$p < 0.0001, §§§p < 0.0001, one-way ANOVA, n = 10 simulations).

(E) SD of mean V_m (spikes removed) for 100% gK_{Ca} + sleep ions, 75% gK_{Ca} + awake ions, or 50% gK_{Ca} + awake ions.

(F) Boxplot for SD of mean V_m for 100% gK_{Ca} + sleep ions, 75% gK_{Ca} + awake ions, or 50% gK_{Ca} + awake ions. Center line is the median, box limits are 25th and 75th percentiles, and whiskers are maximum and minimum values (*p = 0.011, $^{##}$p = 0.0062, §§p = 0.0018, one-way ANOVA, n = 10 simulations).

(G) Mean V_m distribution for 100% gK_{Ca} + sleep ions, 75% gK_{Ca} + awake ions, or 50% gK_{Ca} + awake ions.

See also Figure S4.

To illuminate if changing gK_{Ca} is the most efficient way to induce the awake state, we performed a bifurcation analysis (i.e., gradual change in parameter values). This revealed that the parameter of gK_{Ca} was the most important parameter for creating state change in firing dynamics (Figure S3). Changing the conductance of almost all other channels had very little effect, except for the parameter gCa_V, which also had the potential to create a transition, but this was still less potent than gK_{Ca} (Figure S3).

Overall, these results demonstrate that the K_{Ca} channel most likely plays a dominant role in sleep V_m activity patterns, and inhibiting this channel, assumedly via increased levels of neuromodulators, is sufficient to induce a transition to the awake state. However, decreasing the conductance of this channel by 25% was not sufficient to invoke a full state transition, suggesting a threshold level for when the state is shifted from sleep to wakefulness.

Awake Ion Concentrations Lower the Threshold for Sleep to Awake State Transition

Although changing extracellular ions from sleep to awake concentrations was not in itself sufficient to induce a state transition (Figures 2 and S2), we speculate if awake ions could lower the threshold for invoking the K_{Ca} channel-dependent state change and in this way be permissive and modulatory on state changes (Figure 4A).

To investigate this, we changed the extracellular ions from sleep to awake concentrations while reducing gK_{Ca} to 75% and 50% as in the previous section (Figure 3). In contrast to Figure 3, when we reduced gK_{Ca} to 75% in the presence of awake ions, we observed a state transition with V_m kept in the upstate for long periods and with few downstates (Figure 4B). As before, when reducing gK_{Ca} to 50%, the state change was pronounced, with V_m tonically depolarized and the neuron continuously firing (Figure 4B). We now found a significant reduction in 1–4 Hz delta

power with the combination of 75% gK_{Ca} and awake ions ($p = 0.026$, one-way ANOVA, $n = 10$ simulations), as well as with 50% gK_{Ca} and awake ions ($p < 0.0001$, one-way ANOVA, $n = 10$ stimulations) (Figures 4C and 4D). The prevalence of delta power was significantly smaller with 50% gK_{Ca} compared with 75% gK_{Ca} ($p < 0.0001$, one-way ANOVA, $n = 10$ simulation) (Figure 4D), likely reflecting that wakefulness comprises two states (i.e., quiet awake and active awake) (Crochet and Petersen, 2006; McGinley et al., 2015b). Further supporting a permissive effect of awake ions on the sleep to awake transition was the significant decrease in mean V_m SD from 100% gK_{Ca} and sleep ions (0.81 ± 0.15 mV) to 75% K_{Ca} and awake ions (0.64 ± 0.13 mV) ($p = 0.011$, one-way ANOVA, $n = 10$ simulations). Reducing gK_{Ca} to 50% with awake ions caused a significant decrease in mean V_m SD to (0.51 ± 0.07 mV) ($p = 0.0062$, one-way ANOVA, $n = 10$ simulations), significantly smaller than with 75% gK_{Ca} ($p = 0.0018$, one-way ANOVA, $n = 10$ simulations), again pointing to multiple awake states (Figure 4F). Finally, the mean V_m distribution was shifted toward uni-modality with 75% gK_{Ca} and awake ions, and this was even more apparent with 50% gK_{Ca} and awake ions (Figure 4G).

Taken together, these data suggest that the awake ion concentrations reduce the threshold for invoking a sleep to awake state transition, and thereby are permissive on this state change. We found that $[K^+]_o$ is the most potent mediator of this ion-concentration-mediated effect, but the combined concurrent shift in all three ion species triggers the greatest sleep to awake state change (Figure S4). What is more, the results point to and support current *in vivo* evidence that the awake state comprises multiple sub-states, with differences in delta oscillations and mean V_m dynamics.

Subtle Change in Extracellular Ion Concentrations Shifts the State from Quiet Awake to Active Awake

After demonstrating that the awake ion concentrations are permissive for shifting V_m dynamics from sleep to awake (Figures 4 and S4), we next investigated the two apparent awake states in greater detail, and in particular the role of extracellular ion concentrations on the transition from the quiet awake to active awake state. For this, we speculate that an arousal-related "hyper-awake" ion composition (in addition to the sleep and awake ion compositions) might exist and could be involved in shifting V_m into the active awake state (Bennett et al., 2013; Crochet and Petersen, 2006; Gentet et al., 2010; McGinley et al., 2015a; Polack et al., 2013; Reimer et al., 2014; Zagha et al., 2013). As an estimate, we changed extracellular ions with the same magnitude as observed between sleep and awake for formulating the hypothesized hyper-awake ion concentrations ($[K^+]_o$ = 4.9 mM, $[Ca^{2+}]_o$ = 1.05 mM, and $[Mg^{2+}]_o$ = 0.6 mM) (Figure 4A).

We initially simulated the quiet awake state (75% gK_{Ca} and awake ions) and then selectively shifted the extracellular ion concentrations to hyper-awake ions while maintaining gK_{Ca} at 75% (Figures 5A and 5B). We observed that with awake ions, V_m alternated between long periods of firing (upstate) and occasional silent downstates (Figure 5B), similar to what is described in quiet awake rodents (Crochet and Petersen, 2006; McGinley et al., 2015a; Yamashita et al., 2013). When we shifted to hyper-awake ion concentrations, we observed an annihilation of downstates, and V_m was maintained in the depolarized upstate with continuous firing as a result (Figure 5B). We next analyzed these two V_m states further. We found that with hyper-awake ions, 1–4 Hz delta power significantly decreased ($p = 0.002$, Student's t test, $n = 10$ simulations) and 25–45 Hz gamma power significantly increased ($p = 0.0023$, Student's t test, $n = 10$ simulations) (Figures 5C–5E). This result is similar to what has been observed when rodents transition from the quiet to the active awake state (Niell and Stryker, 2010; Reimer et al., 2014; Vinck et al., 2015). With hyper-awake ions, mean V_m was significantly more depolarized than with awake ions (−49.38 ± 0.11 mV and −52.62 ± 0.23 mV; $p = 0.002$, Student's t test, $n = 10$ simulations) (Figure 5F), keeping V_m closer to the firing threshold. Finally, mean V_m distribution was shifted toward the depolarized upstate with hyper-awake ions, representing the lack of downstates (Figure 5G). All of these results are in congruence with *in vivo* recordings obtained in awake rodents, where the active awake state is characterized by a depolarized V_m and a lack of downstates (Crochet and Petersen, 2006; McGinley et al., 2015a; Yamashita et al., 2013).

Taken together, these results demonstrate that subtle changes in extracellular ion concentrations are sufficient for shifting V_m dynamics from the quiet awake state to the active awake state. Shifting to the hypothesized hyper-awake ion concentrations recapitulated key properties of the active awake state V_m dynamics, including increased gamma oscillations and depolarized V_m. Further analysis revealed that shifting $[K^+]_o$ alone was sufficient for invoking this state transition, but the combined effect of shifting all three ion species was greater (Figure S5), suggesting a biological importance of concerted extracellular ion changes. We advocate that the existence of such hyper-awake ion concentrations should be investigated in future *in vivo* experiments, as well as its ability to causally invoke the proposed awake state changes.

Transitions between Brain States Are Governed by Chaotic Dynamics

After finding that awake ion concentrations are permissive for shifting the state from sleep awake (Figure 4), and that hyper-awake ion concentrations can invoke the transition from quiet to active awake (Figure 5), we next investigated the state-dependent properties of V_m dynamics in more analytical and physical terms, as we altered extracellular ion concentrations.

First, we performed a detailed simulation of the sleep state, where in the deterministic system we found spikes and V_m oscillations to be stable and periodic in the sense that the pattern was self-repeating, and small perturbations in the initial conditions did not make the trajectories diverge (Figure 6A). This therefore had to be a closed trajectory with several small loops that occur when the neuron fires, which is best visualized in a three-dimensional phase space spanned by three variables (V_m, Ca^{2+}, and n_K) (Figure 6B). This means that V_m dynamics in the sleep state is well defined by regular and stable oscillations, exactly as what one would expect from a synchronous system.

Next, we considered which ion currents are most important for changing the state from sleep to awake. From what was observed in the awake state (Figures 3 and 4), we characterize the transition in terms of (1) the rate at which a silent downstate period is initiated, (2) the mean time duration of a spiking upstate period, and

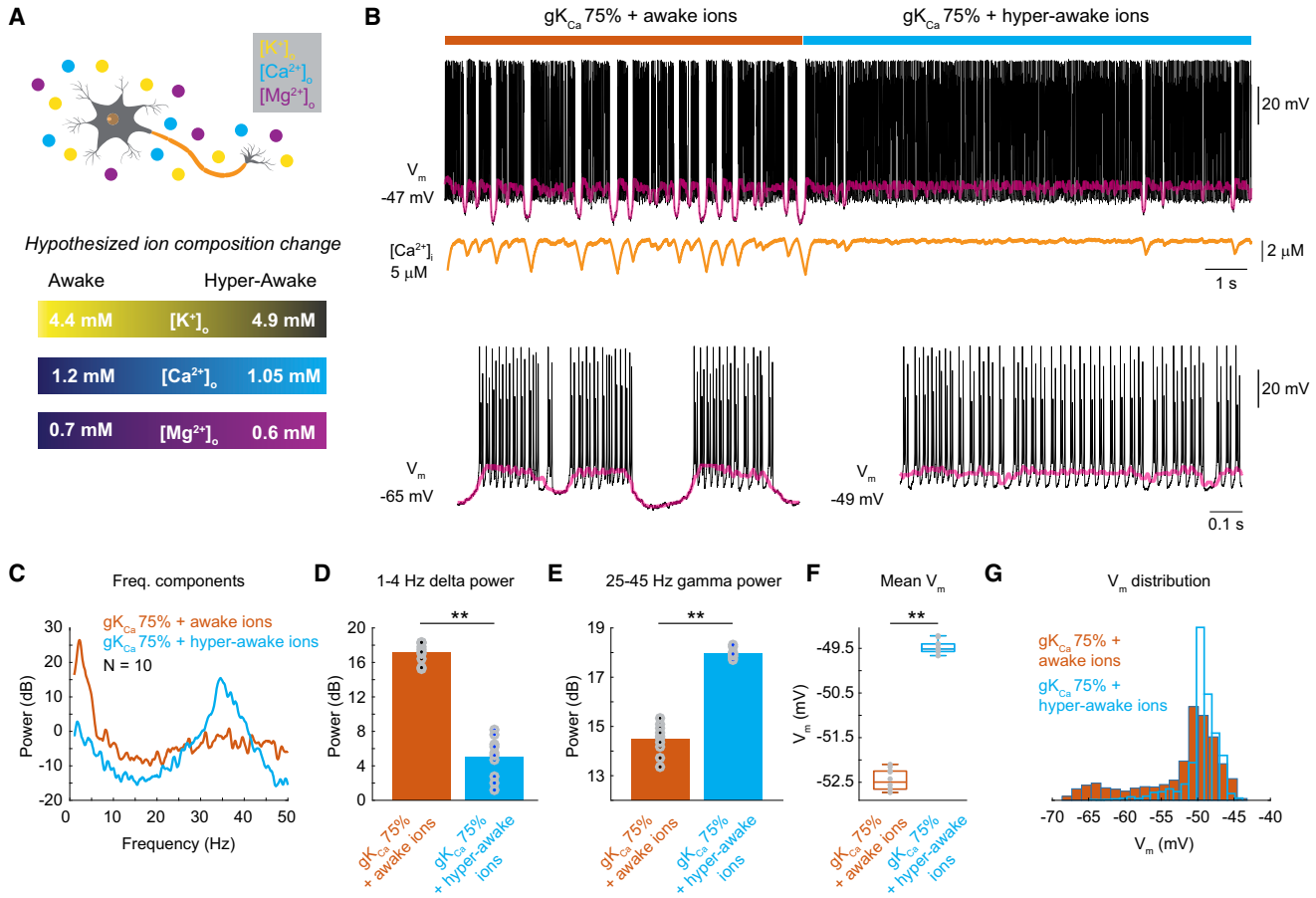

Figure 5. Transition between Two Awake States Can Be Controlled by Extracellular Ion Concentrations

(A) Schematic diagram of hypothesized shift in extracellular ion concentration from awake to hyper-awake. Awake: $[K^+]_o$ = 4.4 mM, $[Ca^{2+}]_o$ = 1.2 mM, and $[Mg^{2+}]_o$ = 0.7 mM. Hyper-awake: $[K^+]_o$ = 4.9 mM, $[Ca^{2+}]_o$ = 1.05 mM, and $[Mg^{2+}]_o$ = 0.6 mM.

(B) Representative membrane potential (V_m), firing pattern, and intracellular Ca^{2+} concentration ($[Ca^{2+}]_i$) with 75% gK_{Ca} + awake ions and 75% gK_{Ca} + hyper-awake ions. Below is an expansion of V_m dynamics.

(C) V_m frequency spectra for 75% gK_{Ca} + awake ions and 75% gK_{Ca} + hyper-awake ions.

(D) 1–4 Hz delta power for 75% gK_{Ca} + awake ions and 75% gK_{Ca} + hyper-awake ions (**p = 0.002, Student's t test, n = 10 simulations).

(E) 25–45 Hz gamma power for 75% gK_{Ca} + awake ions and 75% gK_{Ca} + hyper-awake ions (**p = 0.0023, Student's t test, n = 10 simulations).

(F) Boxplot for mean V_m for 75% gK_{Ca} + awake ions and 75% gK_{Ca} + hyper-awake ions. Center line is the median, box limits are 25th and 75th percentiles, and whiskers are maximum and minimum values (**p = 0.002, Student's t test, n = 10 simulations).

(G) Mean V_m distribution for 75% gK_{Ca} + awake ions and 75% gK_{Ca} + hyper-awake ions.

See also Figure S5.

(3) the SD of this measure. These numbers combined describe much of the change in V_m dynamics that happens between the sleep and awake state. By affecting only one of the currents at a time by the change in extracellular ion concentrations from sleep to awake, we found the largest ion-concentration-mediated effect was produced on the Ca_V-mediated current (Figure 6C). This was even better observed if we combined the sleep to awake ion-mediated changes in Ca_V current with a small perturbation in gK_{Ca} (Figure 6C). Thus, here we found that affecting only the Ca_V channel by changes in sleep to awake ion concentration can account for much of the irregularities of the awake state, and that a similar ion-mediated effect can occur for the extrinsic AMPA receptor, and this induces a big step toward the awake state (Figure 6C). We also show that decreasing gK_{Ca} is the most important factor in moving V_m dynamics toward the awake state, but that changes in extracellular ion concentrations amplify this effect markedly (Figure 6C).

As observed in the sections above, transition from the sleep to the awake state could be invoked by a 25% reduction in gK_{Ca} and a concomitant change to awake ion concentrations (Figure 4). With the combination of 75% gK_{Ca} and awake ions, V_m dynamics are more irregular and significantly long periods of upstates and spiking can occur before a silent downstate is recovered (Figure 4B). This suggests that V_m dynamics in the awake state is chaotic, meaning that the phase space has a strange attractor. Deterministic chaos is defined by the fact that two initial conditions, being infinitesimally perturbed, will have diverging trajectories as time evolves, and that one cycle will never repeat itself and therefore no closed cycles exist on a strange attractor (Lorenz, 1963) (Box 1). We tested this by

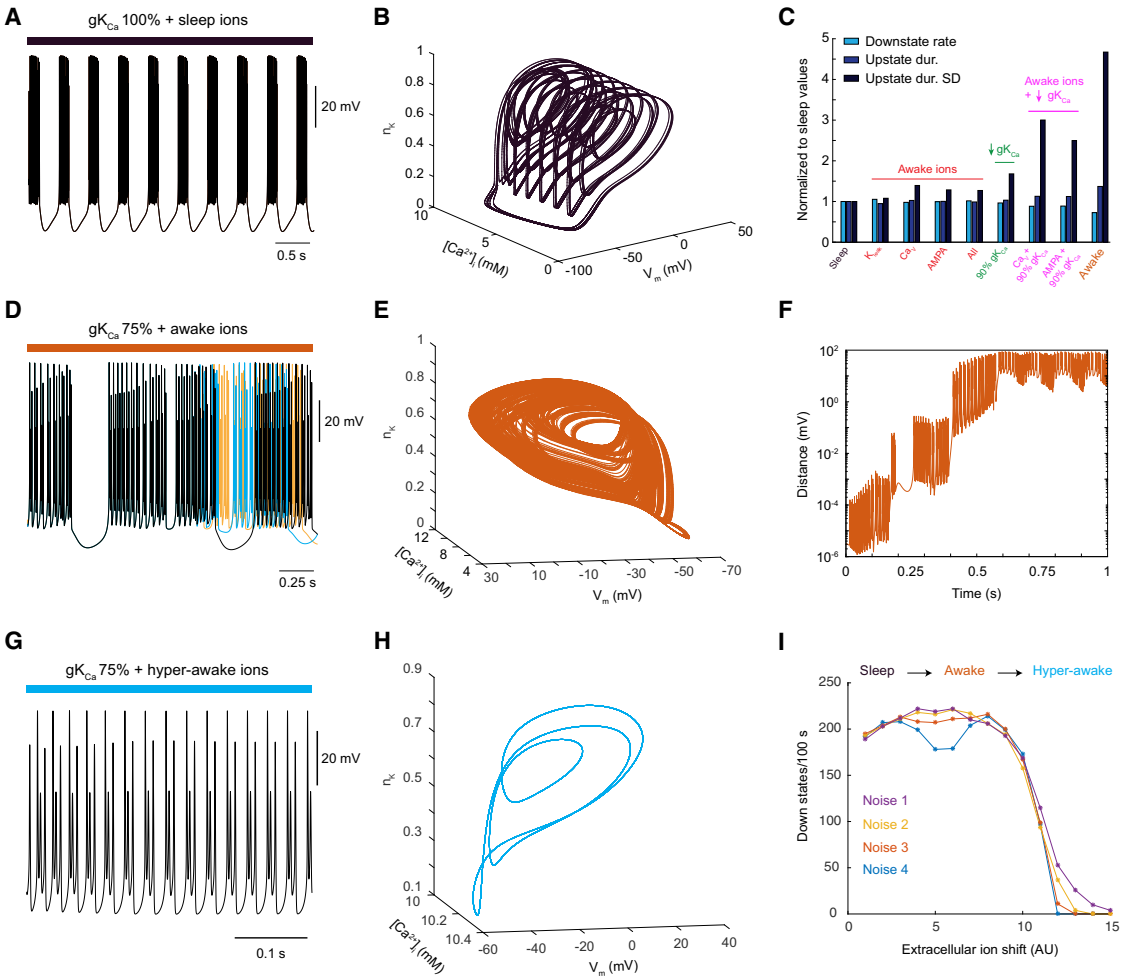

Figure 6. Transition from Sleep to Wakefulness Is Governed by Chaotic Dynamics

(A) Representative membrane potential (V_m) firing pattern in the sleep state with 100% gK_{Ca} and sleep ion composition ($[K^+]_o$ = 3.9 mM, $[Ca^{2+}]_o$ = 1.35 mM, and $[Mg^{2+}]_o$ = 0.8 mM).

(B) Phase space plot showing the trajectory in the sleep state.

(C) Measures for the effect of different ion channel-mediated currents on V_m dynamics. Light blue is the average rate of initiating a silent downstate periods. Blue is the average duration of the spiky upstate periods. Dark blue is the SD in the duration of upstate periods. All measures are normalized to the sleep state.

(D) Representative V_m firing patterns with 75% gK_{Ca}, awake ion composition ($[K^+]_o$ = 4.4 mM, $[Ca^{2+}]_o$ = 1.2 mM, and $[Mg^{2+}]_o$ = 0.7 mM) and 1 mV perturbations showing the development of different trajectories.

(E) Phase space plot showing the trajectory in the awake state with 75% gK_{Ca} and awake ion composition.

(F) Difference between two V_m trajectories in the awake state with 75% gK_{Ca} and awake ion composition.

(G) Representative V_m firing pattern in the awake state with 75% gK_{Ca} and hyper-awake ion composition ($[K^+]_o$ = 4.9 mM, $[Ca^{2+}]_o$ = 1.05 mM, and $[Mg^{2+}]_o$ = 0.6 mM).

(H) Phase space plot showing the trajectory in the awake state with 75% gK_{Ca} and hyper-awake ion composition.

(I) Number of silent periods for a period of 100 s as the values of $[K^+]_o$, $[Ca^{2+}]_o$, and $[Mg^{2+}]_o$ are perturbed linearly from values for the sleep state to values of the active awake state. On the x axis, 1 corresponds to the sleep state and 9 corresponds to the awake state.

perturbing the initial concentration of $[Ca^{2+}]_i$ by only 1 pM (10^{-12}), and even though V_m trajectories are very similar in the beginning, after some seconds they are completely different (Figure 6D). Another way of visualizing the chaotic nature of the awake state V_m dynamics can be seen in Figure 6E, where the trajectory is shown in three dimensions. Here, it seems that the trajectory never repeats and that the dynamics are irregular compared with the regular oscillations in the sleep state. To test if this had the signature of chaos, we calculated the difference in all dimensions between two trajectories and found that they diverge in a complex manner that seems however to be on top of a general exponential diverging, which is what we would expect from a chaotic system (Lorenz, 1963) (Figure 6F).

As shown in previous sections, the sleep to awake state transition that we have now characterized is likely not the end of the story, and an additional active awake state exists (Crochet and Petersen, 2006; McGinley et al., 2015b) (Figures 4 and 5). Furthermore, we hypothesize that a parameter set of hyper-awake ion concentrations exist (Figure 5A). As in Figure 5, we observed that with hyper-awake ions, V_m dynamics is a

Box 1. What Is Chaos?

Chaos is a well-defined mathematical concept that occurs in non-linear dynamical systems with three or more dimensions. It is defined by the property that two initial conditions infinitesimally apart exhibit exponentially diverging trajectories as time evolves. Such systems are deterministic in the sense that if one knows the initial state of the system exactly, then the trajectory will be the same every time it is initiated in that state. Chaos is thus a mathematical definition that should not be confused with the use of chaos in normal language. Furthermore, it is important to distinguish chaos from randomness or stochasticity in general. Randomness normally refers to non-deterministic responses due to stochastic noise, which in principle appears in any system of nature. The effects of stochasticity can sometimes be negligible but may, in some cases, give rise to a different dynamics than seen in a deterministic system. Examples of this can be sustained oscillations or multi-stability. Since systems always exhibit some uncertainty, the initial conditions in a system are never completely known and therefore chaotic systems, from a practical point of view, might appear random since it is impossible to predict the dynamical outcome.

continuously spiking process with no occurrence of silent downstates (Figure 6G), which likely correspond to an aroused and alert active awake state (Crochet and Petersen, 2006; Polack et al., 2013). We find that this state is not chaotic, but rather a well-defined, high-frequency three cycle (Figure 6H). This means that the initial transition from the sleep state can be regarded as a mediator between two robust states (sleep and active awake) defined by closed cycles. We consider it of great importance that the dynamics of V_m changes from sleep to the awake state and even further into an active awake state, using effects of chaotic dynamics, and how these changes are sensitive to subtle changes in extracellular ion concentrations.

Next, we performed the V_m simulation while applying white noise, which in the awake state, with awake ions, gives rise to V_m dynamics as shown in Figure 6D. Since stochasticity is present in every system and intrinsic biological noise is assumed to appear around the ion channels, noise is a very import element in this region where multi-stable solutions seem to arise. Since the most striking difference between the sleep and awake states is the occurrence/lack of silent downstates, we used the number of silent periods as a measure to characterize the gradual transition from sleep to the active awake state. We investigated this for four different noise levels while we linearly perturbed the values of $[K^+]_o$, $[Ca^{2+}]_o$, and $[Mg^{2+}]_o$ from the sleep to the hyper-awake concentrations. As can be observed from Figure 6I, the complete state transition in this measure is a continuous process for the noise levels tested, and shifting extracellular ion concentrations is sufficient to fully transition from the quiet awake to the active awake state.

In summary, we found that the transition from sleep to full wakefulness is modulated by changes in extracellular ion concentrations. Moreover, we show that if extracellular ions change, for instance if $[K^+]_o$ is either below or above 3.9 and 4.5 mM, respectively, the dynamics of the system is determined by a stable limit cycle with several smaller loops included, whereas for $[K^+]_o$ within the range of 3.9 and 4.5 mM, the system is chaotic, which can ensure a smooth and robust transition between the sleep state and the active awake state.

DISCUSSION

Neuronal states powerfully influence sensory processing and perceptions (Harris and Thiele, 2011; Lee and Dan, 2012; Lee et al., 2014; McGinley et al., 2015a; Vinck et al., 2015). Here, we have shown that the concentrations of extracellular ions influence K_{Ca} channel-mediated sleep to awake transitions and can themselves drive the switch from quiet awake to active awake. We demonstrate that the state change from sleep to awake is characterized by the transition from stable to chaotic dynamics, and argue that chaotic dynamics mediates a smooth transition between the quiet awake and active awake state, remarkably robust to intrinsic noise.

Previous studies have causally implicated ion concentrations in sleep to awake transitions (Ding et al., 2016). However, due to the intimate relation between neural activity and ionic changes, causality is difficult to establish *in vivo*. In our model, exclusively shifting ion concentrations by the same magnitude as measured *in vivo* was insufficient to cause a complete sleep to awake state transition (Figures 2, 6C, and S2), suggesting that other parameters need to change in time in order to transition the neuron into to the awake state, and that ion concentration changes are not causal for this state transition. This might seem as an advantageous built-in gate mechanism, since extracellular ion concentrations are affected by even slight changes in neuronal firing (Hounsgaard and Nicholson, 1983; Lux, 1974; Lux and Neher, 1973; Nicholson et al., 1977), and global brain states should be robust to such small ion fluctuations, not causing the system to constantly cycle between sleep and awake.

We determined that decreasing the conductance of the K_{Ca} channel is a powerful way to induce the sleep to awake state change (Figures 3, 6C, and S3), in congruence with previous work implicating this channel as a prime mechanism for V_m downstates (McCormick and Williamson, 1989; McCormick et al., 1993; Steriade et al., 1993; Tatsuki et al., 2016). Shifting to the awake ion concentrations was permissive to decreasing the conductance of the K_{Ca} channel (Figures 4, 6C, and S4), advocating that subtle changes in extracellular ion concentrations can lower the threshold for how much ion channel modulation is required to shift the state. Changing the global environment surrounding neurons, in addition to modulating selective intrinsic ion channels, might be a simple, yet powerful, way to shift the state of entire brain-wide neuronal networks and ultimately for changing the behavioral state.

In more abstract terms, transitions between states in living organisms are fundamental for the functions and complexity of that organism. However, it is often speculated that very rapid state changes might be harmful for cells, since they might not be able to adapt properly and fast enough to the new dynamics. In this regard, the state transition described here for neuronal V_m dynamics has the beneficial property that it represents a gradual

and smooth change between the two stereotypical behavioral states, sleep and wakefulness. Furthermore, the chaotic nature of the phase space even guarantees the smoothness for a range of different intrinsic noise levels, which ensures that neurons can transition between states in a controlled and noise-robust manner when this is needed and appropriate.

It is increasingly appreciated that the awake state is comprised of at least two sub-states, namely quiet awake and active awake, related to the level of arousal and motor behavior (Bennett et al., 2013; Crochet and Petersen, 2006; Gentet et al., 2010; McGinley et al., 2015a; Polack et al., 2013; Reimer et al., 2014; Zagha et al., 2013). Rodent studies have suggested that the ongoing awake state shapes how the brain processes incoming sensory inputs. For example, the gain of visual-evoked responses in the visual cortex is increased when neurons are in the active awake state, whereas auditory responses in the auditory cortex are suppressed (Bennett et al., 2013; McGinley et al., 2015a; Polack et al., 2013; Schneider et al., 2014). This indicates that the brain state powerfully and differentially scales what sensory modalities are up- and downregulated at a given moment in time for optimizing sensory processing and neural computations, making it important to understand at the mechanistic level what determines brain states and the transition between them.

Here, we hypothesized that in addition to sleep and awake extracellular ion concentrations (Ding et al., 2016), a hyper-awake ion composition might exist (Figures 5, 6, and S5). When K_{Ca} was kept partially inhibited (75% gK_{Ca}), shifting from the awake to the hyper-awake ion concentrations produced a state change similar to what is observed when rodents transition from quiet to active (Crochet and Petersen, 2006; Yamashita et al., 2013) (Figures 5, 6, and S5). This ion-mediated state change was characterized by a decrease in delta power, an increase in gamma power, V_m depolarization, and a uni-modal V_m distribution (Figure 5); similar to what has been observed *in vivo* with intracellular recordings from cortical neurons in behaving rodents. We predict that subtle concerted changes in extracellular ion concentrations could be a key mechanism for the rapid and often-occurring state shifts in the awake brain, allowing sensory processing and neural computations to be rapidly modified based on the different situational demands. Whether our hypothesized shifts in extracellular ion concentrations do occur in the awake brain during active behavior and states of elevated arousal, as well as whether this ionic shift is primary or secondary to neural activity, will be interesting and important to resolve in future experiments.

We consider the frequency and length of the silent downstate periods a key signature defining the different dynamics in the two awake states (Figure 6I). It can be argued that in the active awake state, V_m is sustained depolarized and only high-frequency spikes occur, and one might entertain the speculative hypothesis that this is required for rapid responses to incoming barrages of sensory stimuli and for decision making. In this case, one would ideally avoid the hyperpolarized silent downstates and in general slow oscillations in the V_m. From a dynamical systems point of view, this means that the trajectory should not visit a large part of the phase space. Since this is the case for a chaotic system, the fact that the chaotic dynamics disappears in the active awake state can be regarded as a beneficial mechanism that ensures the occurrence of only high-frequency spikes and maintains V_m close to the firing threshold, keeping the neuron in a state for optimal responsiveness to sensory inputs from the periphery. We note that from a theoretical point of view, it is possible to imagine a stable limit cycle that can guarantee a smooth transition. In this picture, the temporal period between downstates gets shorter and shorter as the parameters change in the quiet awake state, for it to completely disappear in the end in the hyper-awake state. However, we believe there are several intriguing elements in a chaotic transition to the awake state in this neuronal state transition. Firstly, since not only one, but several, parameters are changed in the sleep to awake state transition, chaotic dynamics is a clever way for the system to make a path-independent transition between the two states. Due to the never-repeating trajectories, the system does not change significantly if, for example, the changes in $[Ca^{2+}]_o$ occur before $[K^+]_o$ or vice versa. This would normally not be the case for a stable limit cycle, and thus the chaotic transition makes the transition to the awake state change more robust. Secondly, we believe that chaotic dynamics is an important property of neurons in the awake state since one would expect that neurons in this state need the capacity to create a variety of different combinatorial outputs on a population level. If the neuronal dynamics in the awake state were purely stable limit cycles differing in period, small differences in incoming inputs would lead to very small differences in output firing, and thus information encoding. However, since they are governed by chaotic dynamics, the sensitivity to the always existing small perturbations that accompany external stimulation, can lead to a much more complex variety of outcomes that are likely highly important and necessary for higher-order neuronal computations. Thirdly, it is intriguing to imagine that since all neurons are governed by the dynamics of a stable limit cycle in the sleep state, they have the potential to synchronize their firing outputs through their common oscillations. Now, perturbing the system could change the period of oscillations but would not necessarily destroy this activity synchrony between neurons. However, as the awake state is chaotic, this population synchrony would naturally disappear. In this way, the awake state would make each neuron more independent, since it is no longer "bound" by the dynamics of the state, and the specific feature-selective inputs to each neuron can have a great effect on the firing output for that particular neuron in the end.

This work uncovers an important function of extracellular ion concentrations and chaos dynamics in neuronal state transitions that, to the best of our knowledge, has not been previously reported. The transition between global brain states needs to be strictly controlled and well regulated to avoid risky diseases such narcolepsy or insomnia. As we show, the concentration of extracellular ions is a key parameter for neuronal state changes, and these state transitions are governed by chaotic dynamics. Concerted regulation and shifts in ion concentrations therefore expand the toolbox available to the brain for controlling state-dependent activity, and thus need to be considered as an integrated mechanism in future investigations of what determines ongoing activity and state transitions in the brain.

STAR★METHODS

Detailed methods are provided in the online version of this paper and include the following:

- KEY RESOURCES TABLE
- CONTACT FOR REAGENT AND RESOURCE SHARING
- EXPERIMENTAL MODEL AND SUBJECT DETAILS
  - Description of the Extended Averaged-Neuron Model
- METHOD DETAILS
  - Membrane Potential (V_m) Analysis
- DATA AND SOFTWARE AVAILABILITY
  - Software
  - Algorithms
- QUANTIFICATION AND STATISTICAL ANALYSIS
- ADDITIONAL RESOURCES

SUPPLEMENTAL INFORMATION

Supplemental Information includes five figures and can be found with this article online at https://doi.org/10.1016/j.cels.2017.11.011.

ACKNOWLEDGMENTS

M.L.H. and M.H.J. acknowledge support from the Danish Council for Independent Research and Danish National Research Foundation through StemPhys Center of Excellence, grant number DNRF116. R.R. acknowledges support from the European Research Council Starting Grant "CIRCUITASSEMBLY" contract 638730 to Keisuke Yonehara.

AUTHOR CONTRIBUTIONS

Conceptualization, R.R. and M.L.H.; Methodology, R.R., M.H.J., and M.L.H.; Investigation, R.R., M.H.J., and M.L.H.; Writing, R.R. and M.L.H.; Visualization, R.R. and M.L.H.

Received: June 16, 2017
Revised: September 7, 2017
Accepted: November 20, 2017
Published: December 13, 2017

REFERENCES

Amzica, F., Massimini, M., and Manfridi, A. (2002). Spatial buffering during slow and paroxysmal sleep oscillations in cortical networks of glial cells in vivo. J. Neurosci. *22*, 1042–1053.

Bazhenov, M., Timofeev, I., Steriade, M., and Sejnowski, T.J. (2002). Model of thalamocortical slow-wave sleep oscillations and transitions to activated States. J. Neurosci. *22*, 8691–8704.

Bennett, C., Arroyo, S., and Hestrin, S. (2013). Subthreshold mechanisms underlying state-dependent modulation of visual responses. Neuron *80*, 350–357.

Chen, J.-Y., Chauvette, S., Skorheim, S., Timofeev, I., and Bazhenov, M. (2012). Interneuron-mediated inhibition synchronizes neuronal activity during slow oscillation. J. Physiol. *590*, 3987–4010.

Compte, A., Sanchez-Vives, M.V., McCormick, D.A., and Wang, X.-J. (2003). Cellular and network mechanisms of slow oscillatory activity and wave propagations in a cortical network model. J. Neurophysiol. *89*, 2707–2725.

De Col, R., Messlinger, K., and Carr, R.W. (2008). Conduction velocity is regulated by sodium channel inactivation in unmyelinated axons innervating the rat cranial meninges. J. Physiol. *586*, 1089–1103.

Crochet, S., and Petersen, C.C.H. (2006). Correlating whisker behavior with membrane potential in barrel cortex of awake mice. Nat. Neurosci. *9*, 608–610.

Diarra, A., Sheldon, C., and Church, J. (2001). In situ calibration and [H^+] sensitivity of the fluorescent Na+ indicator SBFI. Am. J. Physiol. Cell Physiol. *280*, C1623–C1633.

Dietzel, I., Heinemann, U., Hofmeier, G., and Lux, H.D. (1982). Stimulus-induced changes in extracellular Na^+ and C^{l-} concentration in relation to changes in the size of the extracellular space. Exp. Brain Res. *46*, 73–84.

Ding, F., O'Donnell, J., Xu, Q., Kang, N., Goldman, N., and Nedergaard, M. (2016). Changes in the composition of brain interstitial ions control the sleep-wake cycle. Science *352*, 550–555.

Enger, R., Tang, W., Vindedal, G.F., Jensen, V., Johannes Helm, P., Sprengel, R., Looger, L.L., and Nagelhus, E.A. (2015). Dynamics of ionic shifts in cortical spreading depression. Cereb. Cortex *25*, 4469–4476.

Fröhlich, F., Bazhenov, M., Timofeev, I., Steriade, M., and Sejnowski, T.J. (2006). Slow state transitions of sustained neural oscillations by activity-dependent modulation of intrinsic excitability. J. Neurosci. *26*, 6153–6162.

Fröhlich, F., Bazhenov, M., Iragui-Madoz, V., and Sejnowski, T.J. (2008). Potassium dynamics in the epileptic cortex: new insights on an old topic. Neuroscientist *14*, 422–433.

Gentet, L.J., Avermann, M., Matyas, F., Staiger, J.F., and Petersen, C.C.H. (2010). Membrane potential dynamics of GABAergic neurons in the barrel cortex of behaving mice. Neuron *65*, 422–435.

Grafstein, B. (1956). Mechanism of spreading cortical depression. J. Neurophysiol. *19*, 154–171.

Harris, K.D., and Thiele, A. (2011). Cortical state and attention. Nat. Rev. Neurosci. *12*, 509–523.

Hill, S., and Tononi, G. (2005). Modeling sleep and wakefulness in the thalamocortical system. J. Neurophysiol. *93*, 1671–1698.

Hounsgaard, J., and Nicholson, C. (1983). Potassium accumulation around individual Purkinje cells in cerebellar slices from the Guinea-pig. J. Physiol. *340*, 359–388.

Jensen, M.S., and Yaari, Y. (1997). Role of intrinsic burst firing, potassium accumulation, and electrical coupling in the elevated potassium model of hippocampal epilepsy. J. Neurophysiol. *77*, 1224–1233.

Krishnan, G.P., Filatov, G., Shilnikov, A., and Bazhenov, M. (2015). Electrogenic properties of the Na^+/K^+ ATPase control transitions between normal and pathological brain states. J. Neurophysiol. *113*, 3356–3374.

Lee, S.H., and Dan, Y. (2012). Neuromodulation of brain states. Neuron *76*, 209–222.

Lee, A.M., Hoy, J.L., Bonci, A., Wilbrecht, L., Stryker, M.P., and Niell, C.M. (2014). Identification of a brainstem circuit regulating visual cortical state in parallel with locomotion. Neuron *83*, 455–466.

Lorenz, E.N. (1963). Deterministic nonperiodic flow. J. Atmos. Sci. *20*, 130–141.

Lux, H.D. (1974). Fast recording ion specific microelectrodes: their use in pharmacological studies in the CNS. Neuropharmacology *13*, 509–517.

Lux, H.D., and Neher, E. (1973). The equilibration time course of $[K^+]_o$ in cat cortex. Exp. Brain Res. *17*, 190–205.

Markova, O., Mukhtarov, M., Real, E., Jacob, Y., and Bregestovski, P. (2008). Genetically encoded chloride indicator with improved sensitivity. J. Neurosci. Methods *170*, 67–76.

Mayer, M.L., Westbrook, G.L., and Guthrie, P.B. (1984). Voltage-dependent block by Mg^{2+} of NMDA responses in spinal cord neurones. Nature *309*, 261–263.

McCormick, D.A., and Williamson, A. (1989). Convergence and divergence of neurotransmitter action in human cerebral cortex. Proc. Natl. Acad. Sci. USA *86*, 8098–8102.

McCormick, D.A., Wang, Z., and Huguenard, J. (1993). Neurotransmitter control of neocortical neuronal activity and excitability. Cereb. Cortex *3*, 387–398.

McGinley, M.J., David, S.V., and McCormick, D.A. (2015a). Cortical membrane potential signature of optimal states for sensory signal detection. Neuron *87*, 179–192.

McGinley, M.J., Vinck, M., Reimer, J., Batista-Brito, R., Zagha, E., Cadwell, C.R., Tolias, A.S., Cardin, J.A., and McCormick, D.A. (2015b). Waking state:

rapid variations modulate neural and behavioral responses. Neuron *87*, 1143–1161.

Mitra, P., and Bokel, H. (2008). Observed Brain Dynamics (Oxford University Press).

Nicholson, C., Bruggencate, G.T., Steinberg, R., and Stöckle, H. (1977). Calcium modulation in brain extracellular microenvironment demonstrated with ion-selective micropipette. Proc. Natl. Acad. Sci. USA *74*, 1287–1290.

Niell, C.M., and Stryker, M.P. (2010). Modulation of visual responses by behavioral state in mouse visual cortex. Neuron *65*, 472–479.

Nowak, L., Bregestovski, P., Ascher, P., Herbet, A., and Prochiantz, A. (1984). Magnesium gates glutamate-activated channels in mouse central neurones. Nature *307*, 462–465.

Orkand, R.K., Nicholls, J.G., and Kuffler, S.W. (1966). Effect of nerve impulses on the membrane potential of glial cells in the central nervous system of amphibia. J. Neurophysiol. *29*, 788–806.

Polack, P.O., Friedman, J., and Golshani, P. (2013). Cellular mechanisms of brain state–dependent gain modulation in visual cortex. Nat. Neurosci. *16*, 1331–1339.

Raimondo, J., Joyce, B., Kay, L., Schlagheck, T., Newey, S.E., Srinivas, S., and Akerman, C.J. (2013). A genetically-encoded chloride and pH sensor for dissociating ion dynamics in the nervous system. Front. Cell. Neurosci. *7*, 202.

Rasmussen, R., Nedergaard, M., and Petersen, N.C. (2016). Sulforhodamine 101, a widely used astrocyte marker, can induce cortical seizure-like activity at concentrations commonly used. Sci. Rep. *6*, 30433.

Reimer, J., Froudarakis, E., Cadwell, C.R., Yatsenko, D., Denfield, G.H., and Tolias, A.S. (2014). Pupil fluctuations track fast switching of cortical states during quiet wakefulness. Neuron *84*, 355–362.

Rose, C.R., and Konnerth, A. (2001). NMDA receptor-mediated Na^+ signals in spines and dendrites. J. Neurosci. *21*, 4207–4214.

Rose, C.R., and Ransom, B.R. (1996). Intracellular sodium homeostasis in rat hippocampal astrocytes. J. Physiol. *491* (Pt 2), 291–305.

Sanchez-Vives, M.V., Mattia, M., Compte, A., Perez-Zabalza, M., Winograd, M., Descalzo, V.F., and Reig, R. (2010). Inhibitory modulation of cortical up states. J. Neurophysiol. *104*, 1314–1324.

Schneider, D.M., Nelson, A., and Mooney, R. (2014). A synaptic and circuit basis for corollary discharge in the auditory cortex. Nature *513*, 189–194.

Shih, P.Y., Savtchenko, L.P., Kamasawa, N., Dembitskaya, Y., McHugh, T.J., Rusakov, D.A., Shigemoto, R., and Semyanov, A. (2013). Retrograde synaptic signaling mediated by K^+ efflux through postsynaptic NMDA receptors. Cell Rep. *5*, 941–951.

Somjen, G.G. (2001). Mechanisms of spreading depression and hypoxic spreading depression-like depolarization. Physiol. Rev. *81*, 1065–1096.

Somjen, G.G. (2002). Ion regulation in the brain: implications for pathophysiology. Neuroscientist *8*, 254–267.

Somjen, G.G. (2004). Ions in the Brain: Normal Function, Seizures, and Stroke (Oxford University Press).

Steriade, M., Amzica, F., and Nuñez, A. (1993). Cholinergic and noradrenergic modulation of the slow (approximately 0.3 Hz) oscillation in neocortical cells. J. Neurophysiol. *70*, 1385–1400.

Steriade, M., Timofeev, I., and Grenier, F. (2001). Natural waking and sleep states: a view from inside neocortical neurons. J. Neurophysiol. *85*, 1969–1985.

Tagluk, M.E., and Tekin, R. (2014). The influence of ion concentrations on the dynamic behavior of the Hodgkin–Huxley model-based cortical network. Cogn. Neurodyn. *8*, 287–298.

Tatsuki, F., Sunagawa, G.A., Shi, S., Susaki, E.A., Yukinaga, H., Perrin, D., Sumiyama, K., Ukai-Tadenuma, M., Fujishima, H., Ohno, R., et al. (2016). Involvement of Ca^{2+}-dependent hyperpolarization in sleep duration in mammals. Neuron *90*, 70–85.

Timofeev, I., Grenier, F., Bazhenov, M., Sejnowski, T.J., and Steriade, M. (2000). Origin of slow cortical oscillations in deafferented cortical slabs. Cereb. Cortex *10*, 1185–1199.

Traynelis, S.F., and Dingledine, R. (1988). Potassium-induced spontaneous electrographic seizures in the rat hippocampal slice. J. Neurophysiol. *59*, 259–276.

Vinck, M., Batista-Brito, R., Knoblich, U., and Cardin, J.A. (2015). Arousal and locomotion make distinct contributions to cortical activity patterns and visual encoding. Neuron *86*, 740–754.

Yamashita, T., Pala, A., Pedrido, L., Kremer, Y., Welker, E., and Petersen, C.C. (2013). Membrane potential dynamics of neocortical projection neurons driving target-specific signals. Neuron *80*, 1477–1490.

Zagha, E., Casale, A.E., Sachdev, R.N., McGinley, M.J., and McCormick, D.A. (2013). Motor cortex feedback influences sensory processing by modulating network state. Neuron *79*, 567–578.

STAR★METHODS

KEY RESOURCES TABLE

REAGENT or RESOURCE	SOURCE	IDENTIFIER
Software and Algorithms		
Simulations made in c++	This Paper	
MATLAB 6.1	The MathWorks Inc. 2010	https://se.mathworks.com/products/matlab/
Chronux 2.0 Toolbox	Chronux	https://chronux.org/
fcn, d02cjx and d02cjw library packages in Fortran	The NAG Library, The Numerical Algorithms Group (NAG), Oxford, United Kingdom	www.nag.com

CONTACT FOR REAGENT AND RESOURCE SHARING

Further information and requests for resources should be directed to and will be fulfilled by the Lead Contact, Mathias L. Heltberg (heltberg@nbi.ku.dk).

EXPERIMENTAL MODEL AND SUBJECT DETAILS

Description of the Extended Averaged-Neuron Model

We consider the membrane potential (V_m) given by:

$$\frac{dV}{dt} = -\frac{1}{C}\left(\sum I_{Ext}\right) - \frac{1}{AC}\left(\left(\sum I_{Int}\right)\right)$$

$$\text{intrinsic} \in \left[Leak, Na_V, K_V, K_{A-type}, K_{SI}, Ca_V, K_{Ca}, NaP, K_{IR}\right]$$

$$\text{extrinsic} \in [NMDA, AMPA, GABA_A]$$

The units on the left side is mV/ms, but the extrinsic currents are in units of uA whereas the intrinsic currents are in nA, and therefore the first should be multiplied by 1000. This reduces to 10, since we multiply with A, that should be in cm^2 and should thus be divided by 100.

Intrinsic Channel Conductances

For the leak channel we have:

$$I_{Leak} = g_{Leak}(V - V_{Leak})$$

$$g_{Leak} = 0.03573\ mS/cm^2 \quad V_{Leak} = \frac{RT}{zF}\ln\left(\frac{p_K[K]_o + p_{Na}[Na]_o + p_{Cl}[Cl]_i}{p_K[K]_i + p_{Na}[Na]_i + p_{Cl}[Cl]_o}\right) \qquad \text{(Equation 1)}$$

$$R = 8.314472\ J/K/mol \quad T = 310\ kelvins \quad z = valence_{ion} \quad F = 9.64853399x10^4\ C/mol$$

For the voltage-gated sodium channel we have:

$$I_{Na_V} = g_{Na_V} m_{Na_V}^3 h_{Na_V}(V - V_{Na})$$

$$m_{Na_V} = \frac{\alpha_m}{\alpha_m + \beta_m} \qquad \begin{cases} \alpha_m = 0.1\dfrac{V+33}{1-e^{-(V+33)/10}} \\ \beta_m = 4e^{-(V+53.7)/12} \end{cases}$$

$$\dot{h}_{Na_V} = 4\left(\alpha_h\left(1 - h_{Na_V}\right) - \beta_h h_{Na_V}\right) \qquad \begin{cases} \alpha_h = 0.07e^{-(V+50)/10} \\ \beta_h = \dfrac{1}{1+e^{-(V+20)/10}} \end{cases} \qquad \text{(Equation 2)}$$

$$g_{Na_V} = 12.2438\ mS/cm^2 \quad V_{Na} = \frac{RT}{zF}\ln\left(\frac{[Na]_o}{[Na]_i}\right)$$

For the voltage-gated potassium channel we have:

$$I_{K_V} = g_{K_V} n_K^4 (V - V_K)$$

$$\dot{n}_{K_V} = 4\left(\alpha_h\left(1 - h_{K_V}\right) - \beta_h h_{K_V}\right) \quad \begin{cases} \alpha_n = 0.01\dfrac{V+34}{1-e^{-(V+34)/10}} \\ \beta_n = 0.125e^{-(V+44)/25} \end{cases}$$

$$g_{K_V} = 2.61868\ mS/cm^2 \quad V_K = \frac{RT}{zF}\ln\left(\frac{[K]_o}{[K]_i}\right)$$

(Equation 3)

For the fast A-type potassium channel we have:

$$I_{A-type} = g_{A-type} m_{A-type}^3 h_{A-type} (V - V_K)$$

$$m_{A-type} = \frac{1}{1+e^{-(V+50)/20}}$$

$$\dot{h}_{A-type} = \frac{h_{A-type\infty} - h_A - type}{\tau_{hA-type}}$$

$$h_{A-type\infty} = \frac{1}{1+e^{(V+80)/6}}$$

$$g_{A-type} = 1.79259\ mS/cm^2 \quad \tau_{hA-type} = 15ms \quad V_K = \frac{RT}{zF}\ln\left(\frac{[K]_o}{[K]_i}\right)$$

(Equation 4)

For the slowly inactivating potassium channel we have:

$$I_{K_{SI}} = g_{K_{SI}} m_{K_{SI}} (V - V_K)$$

$$m_{K_{SI}} = \frac{h_{m_{K_{SI}\infty}} - m_{K_{SI}}}{\tau_{mK_{SI}}}$$

$$m_{K_{SI}\infty} = \frac{1}{1+e^{-(V+34)/6.6}}$$

$$\tau_{mK_{SI}} = \frac{8}{e^{-(V+55)/30} + e^{(V+55)/30}}$$

$$g_{K_{SI}} = 0.0350135\ mS/cm^2 \quad V_K = \frac{RT}{zF}\ln\left(\frac{[K]_o}{[K]_i}\right)$$

(Equation 5)

For the voltage-gated calcium channel we have:

$$I_{Ca_V} = g_{Ca_V} m_{Ca_V\infty}^2 (V - V_{Ca})$$

$$m_{Ca_V\infty} = \frac{1}{1+e^{(V+20)/9}}$$

$$g_{Ca_V} = 0.0256867\ mS/cm^2 \quad V_{Ca} = \frac{RT}{zF}\ln\left(\frac{[Ca]_o}{[Ca]_i}\right)$$

(Equation 6)

For the calcium-dependent potassium channel we have:

$$I_{K_{Ca}} = g_{K_{Ca}} m_{K_{Ca}\infty} (V - V_K)$$

$$m_{K_{Ca}\infty} = \frac{1}{1+\dfrac{K_D^{3.5}}{[Ca]_i}}$$

$$\left[\dot{Ca}\right]_i = -\alpha_{Ca}(10 \cdot AI_{Ca} + I_{NMDA}) - \frac{[Ca]_i}{\tau_{Ca}}$$

$$g_{K_{Ca}} = 2.34906\ mS/cm^2 \quad K_D = 30\mu M \quad \tau_{Ca} = 121.403ms \quad V_K = \frac{RT}{zF}\ln\left(\frac{[K]_o}{[K]_i}\right)$$

(Equation 7)

For the persistent sodium channel we have:

$$I_{NaP} = g_{NaP} m_{NaP\infty} (V - V_{Na})$$
$$m_{NaP\infty} = \frac{1}{1 + e^{-(V+55.7)/7.7}}$$
$$g_{NaP} = 0.0717984 \ mS/cm^2 \quad V_{Na} = \frac{RT}{zF} \ln\left(\frac{[Na]_o}{[Na]_i}\right) \qquad \text{(Equation 8)}$$

For the inwardly rectifying potassium channel we have:

$$I_{K_{IR}} = g_{K_{IR}} h_{K_{IR}\infty} (V - V_K)$$
$$h_{K_{IR}\infty} = \frac{1}{1 + e^{(V+75)/4}}$$
$$g_{K_{IR}} = 0.0166454 \ mS/cm^2 \quad V_K = \frac{RT}{zF} \ln\left(\frac{[K]_o}{[K]_i}\right) \qquad \text{(Equation 9)}$$

Extrinsic Channel Conductances

We start by defining the saturating function

$$f(V) = \frac{1}{1 + e^{-(V-20)/2)}}$$

We now consider the AMPA receptor:

$$I_{AMPA} = g_{AMPA} s_{AMPA} (V - V_{AMPA})$$
$$\dot{s}_{AMPA} = 3.48 f(V) - \frac{s_{AMPA}}{\tau_{AMPA}}$$
$$g_{AMPA} = 0.513425 \ \mu S/cm^2 \quad V_{AMPA} = \frac{RT}{zF} \ln\left(\frac{p_K[K]_o + p_{Na}[Na]_o}{p_K[K]_i + p_{Na}[Na]_i}\right) \qquad \text{(Equation 10)}$$

For the NMDA receptor we have:

$$I_{NMDA} = \frac{1.1}{1.0 + [Mg]_o / 8.0mM} g_{NMDA} s_{NMDA} (V - V_{NMDA})$$
$$\dot{s}_{NMDA} = 0.5 x_{NMDA} (1 - s_{NMDA}) - \frac{s_{NMDA}}{\tau_{sNMDA}}$$
$$\dot{x}_{NMDA} = 3.48 f(V) - \frac{x_{NMDA}}{\tau_{xNMDA}}$$
$$g_{NMDA} = 0.00434132 \ \mu S/cm^2 \quad V_{NMDA} = \frac{RT}{zF} \ln\left(\frac{p_K[K]_o + p_{Na}[Na]_o + p_{Ca}[Ca]_o}{p_K[K]_i + p_{Na}[Na]_i + p_{Ca}[Ca]_i}\right) \qquad \text{(Equation 11)}$$

For the $GABA_A$ receptor we have:

$$I_{GABA_A} = g_{GABA_A} s_{GABA_A} (V - V_{GABA})$$
$$\dot{s}_{GABA_A} = f(V) - \frac{s_{GABA_A}}{\tau_{sGABA_A}}$$
$$g_{GABA_A} = 0.00252916 \ \mu S/cm^2 \quad V_{GABA} = \frac{RT}{zF} \ln\left(\frac{[Cl]_i}{[Cl]_o}\right) \qquad \text{(Equation 12)}$$

Ion Concentrations

We used the following intra- and extracellular ion concentrations:

$$[Na]_o = 140 \ mM \quad [Na]_i = 7 \ mM$$
$$[K]_o = [3.5; 3.9; 4.4; 4.9; 8; 14] \ mM \quad [K]_i = 7 \ mM$$
$$[Ca]_o = [1.05; 1.2; 1.35] \ mM \quad [Ca]_i = -\alpha_{Ca}(10 \cdot AI_{Ca} + I_{NMDA}) - \frac{[Ca]i}{\tau_{Ca}} \ \mu M$$
$$[Cl]_o = 140 \ mM \quad [Cl]_i = 10 \ mM$$
$$[Mg]_o = [0.6; 0.7; 0.8] \ mM$$

METHOD DETAILS

Membrane Potential (V_m) Analysis

V_m frequency component analysis was performed using procedures in MATLAB similar to previously described (Rasmussen et al., 2016). For exploring frequency-domain dynamics we used the *mtspectrumc* function, a multi-taper method implemented in the Chronux 2.0 toolbox, an open-source, MATLAB-based toolbox available at http://chronux.org/ (Mitra and Bokel, 2008). For this analysis we used a padding factor of 2, time-bandwidth product of 3 and 5 tapers. For determining power content we used the *bandpower* function and afterwards the *pow2db* functions in MATLAB. All power measurements are reported in units of decibel unless otherwise stated. For removing spikes from the simulated V_m, yielding the mean V_m, we median filtered the raw V_m (window size: 80 ms). V_m standard deviation was determined over a 200 ms moving window.

DATA AND SOFTWARE AVAILABILITY

Software

All simulations were performed using scripts written in Fortran, C++ and MATLAB. All data-analysis were performed from scripts written in MATLAB and python using the ROOT software. Figures were composed in Adobe Illustrator. All scripts used for simulation and data analysis from the model, will be available upon reasonable request to Mathias L. Heltberg (heltberg@nbi.ku.dk).

Algorithms

All deterministic simulations were performed using the fcn, d02cjx and d02cjw library packages in Fortran and tested by a similar script written in c++. All stochastic simulations were performed by scripts written in c++, and using the Mersenne Twister to draw random numbers.

QUANTIFICATION AND STATISTICAL ANALYSIS

Statistical testing was carried out in MATLAB. All group comparisons were performed using two-sided parametric paired Student's t test. For comparisons of multiple groups the parametric repeated measures One-way ANOVA with a Geisser-Greenhouse correction and a Dunnett's multiple comparisons correction was used. Lower-case 'n' refers to the number of simulations and is noted in the manuscript text, figure legends and on figure panels whenever appropriate. Statistical significance was considered with P-values less than 0.05. When a statistical test was used, the precise P-value is noted in the manuscript text, and depicted in figures with asterisks: * $P < 0.05$, ** $P < 0.01$, *** $P < 0.001$.

ADDITIONAL RESOURCES

The custom code for the extended Averaged-Neuron model is publicly available online at https://github.com/Neurune/IonsAndChaos.